Check for updates

AGU ADVANCING EARTH AND SPACE SCIENCE

Water Resources Research®

RESEARCH ARTICLE
10.1029/2021WR029902

Suspended Sediment Concentration Profile in a *Typha Latifolia* Canopy

Yuan Xu[1,2] **and Heidi Nepf**[2]

[1]State Key Laboratory of Hydroscience and Engineering, Tsinghua University, Beijing, China, [2]Department of Civil and Environmental Engineering, MIT, Cambridge, MA, USA

Key Points:

- Profiles of suspended sediment concentration (SSC) were measured in a model canopy of *Typha latifolia*
- The vertical turbulent diffusivity depends on plant-generated turbulence and morphology
- A model to predict vertical diffusivity was developed, validated, and used to simulate the SSC with a random displacement model

Supporting Information:

Supporting Information may be found in the online version of this article.

Correspondence to:

Y. Xu,
xuyuan18@mails.tsinghua.edu.cn

Citation:

Xu, Y., & Nepf, H. (2021). Suspended sediment concentration profile in a *Typha Latifolia* Canopy. *Water Resources Research*, *57*, e2021WR029902. https://doi.org/10.1029/2021WR029902

Received 1 MAR 2021
Accepted 29 AUG 2021

© 2021. American Geophysical Union. All Rights Reserved.

Abstract The transport of sediment in regions with vegetation plays an important role in aquatic ecosystems and landform evolution in river deltas. In this study, flow parameters and suspended sediment concentration (SSC) within an emergent canopy with real plant morphology (*Typha latifolia*) were measured in a laboratory channel. *T. latifolia* is a common marsh species with multiple thin leaves emerging from a tight bundle (culm) at the bed. The observed equilibrium SSC profile differed significantly from a Rouse profile, the classic model for SSC over bare beds. The vertical distribution of SSC was nearly uniform in the culm region of the canopy, and decreased with height in the upper canopy region of distributed leaves. The profile of SSC reflected the vertically nonuniform turbulent diffusion, which arose from the plant morphology. A diffusivity model based on cylinder arrays was first validated with tracer data and then adapted to the *T. latifolia* morphology, providing a way to model turbulent diffusivity in marsh systems. The diffusivity model was successfully used within a random displacement model to predict the spatial evolution and equilibrium SSC profile within the *T. latifolia* canopy.

1. Introduction

Aquatic vegetation provides important ecosystem services in rivers, lakes, wetlands, and coastal regions. It protects riverbanks and shorelines from floods and waves, provides shelter for aquatic organisms, enhances water quality, and promotes soil carbon accretion (e.g., Barbier et al., 2011; Costanza et al., 1997; Fourqurean et al., 2012; Kemp et al., 2000). During the past decades, a significant marsh and mangrove area has been lost from river deltas, diminishing these ecosystem services, so there is a growing interest in restoring and managing these systems (e.g., Mississippi River Delta and Mekong Delta; Minderhoud et al., 2019; Nittrouer et al., 2012). To guide restoration, it is necessary to understand the interaction between flow, vegetation, and sediment transport. This study considers the suspended sediment.

In bare channels, the highest suspended sediment concentration (SSC) occurs at the bed, associated with bed-generated turbulence and bed-shear stress (Jiménez, 2012). Turbulent diffusion carries the sediment away from the bed (positive z direction), until an equilibrium is reached between the upward diffusive flux and downward settling flux. This equilibrium is described by the Rouse profile, which has a maximum SSC at the bed (Coleman, 1986; Rouse, 1937). In an array of emergent cylinders, Lu (2008) found that the SSC profile was similar to that observed in a bare channel, decreasing from a maximum at the bed. By assuming a constant vertical diffusivity, Lu (2008) obtained an analytical solution for SSC, which agreed with the experimental data. Similarly, Huai et al. (2019) predicted the SSC profiles in the experiment of Lu (2008) assuming a uniform diffusivity in a random displacement model (RDM). The assumption of a vertically uniform diffusivity is appropriate over most of the water depth within a uniform cylinder array (e.g., Lightbody & Nepf, 2006; Nepf, 1999; Nepf et al., 1997). Tseng and Tinoco (2020) noted that the diffusivity is elevated in a thin boundary layer close to the bed and used this to develop a two-region model to predict the SSC profile in a cylinder array. However, real vegetation has a morphology distinct from uniform cylinders, which can produce a significant vertical variation in velocity and turbulence (Tinoco, 2011; Xu & Nepf, 2020; Zhang et al., 2021), which, in turn, will impact the SSC profile. For example, Li et al. (2020) observed a maximum SSC at the top of a submerged plastic canopy, not at the bed, and this was attributed to elevated turbulence, and thus diffusivity, associated with the shear-layer at the top of a submerged canopy. Similarly, Huai et al. (2019) predicted the SSC profiles measured with a submerged array of cylinders using a diffusivity model that represented the shear-layer turbulence. Vertical variation in emergent vegetation morphology will similarly impact the vertical distribution of turbulence, diffusivity, and SSC. Combining measurements

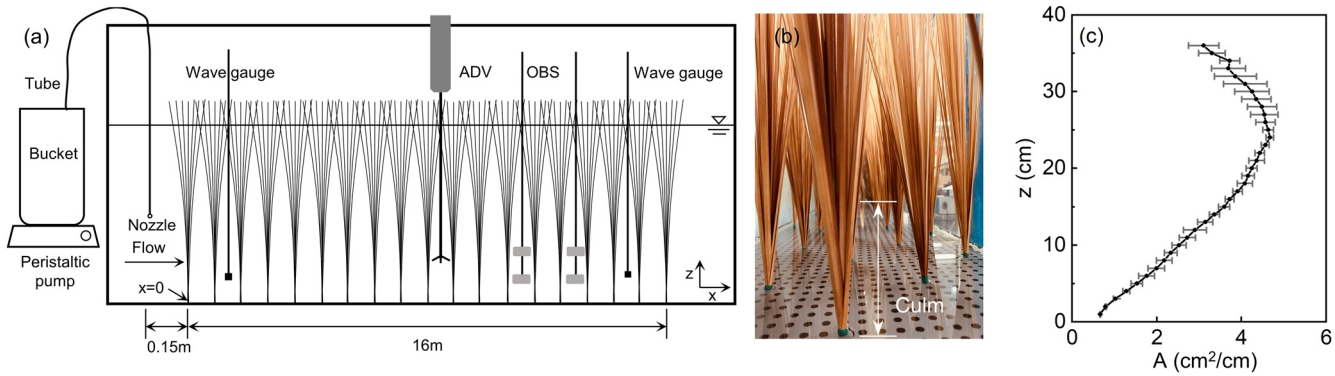

Figure 1. (a) Side view of the channel. Not to scale. Flow is from left to right, with $x = 0$ at the leading edge of canopy, which was 16 m long. Particles were released from a nozzle upstream of the canopy. Velocity was measured with an Acoustic Doppler Velocimeter. The suspended sediment concentration was measured with four optical backscatter sensors, mounted in pairs on two vertical rods. (b) Photo of the *T. latifolia* canopy. (c) *T. latifolia* frontal area per cm vertical interval, A (cm^2/cm) (from Xu & Nepf, 2020).

and simulations of SSC, the present study considered these dependences for the marsh plant *Typha latifolia*, which has multiple thin leaves emerging from a tight culm at the bed (Figure 1).

2. Methods

2.1. Experimental Setup

The experiments were conducted in a 24-m long, 38-cm wide recirculating flume with zero bed slope (Figure 1a). The model plant, *Typha latifolia*, consisted of long sword-shaped leaves, which were bundled into a culm at the base (Figure 1b). Each plastic plant consisted of 40 leaves, with lengths $l_1 = 30$–40 cm and widths $w_1 = 0.1$–0.4 cm, which was the same as real *T. latifolia* leaves (Liu et al., 2017). The plants were placed in a staggered arrangement in PVC baseboards (Figure 1b). Once installed, the canopy height was 38 ± 2 cm. The length (L) and width (W) of the canopy was 16 and 0.38 m, respectively. The area density, m, was 119 plants/m^2, and the depth-average solid volume fraction was $\phi = 0.0057$ to 0.0065, depending on the depth. Plant characteristics are shown in Table 1. Importantly, unlike a cylinder array, the *T. latifolia* canopy was vertically nonuniform. Figure 1c shows the vertical profiles of the plant frontal area per cm vertical interval, A (cm^2/cm), which displays the vertical nonuniformity of *T. latifolia*. Due to this nonuniformity, the depth-average frontal area per volume $\langle a \rangle_z = mA_f / H$, in which A_f is the cumulative frontal area of one plant, $A_f = \int_0^H A dz$, varied with water depth (Table 1).

The inlet to the channel was located 2 m upstream of the canopy, and the flow was controlled by a variable speed pump. The flow rate was monitored by an electromagnetic flowmeter mounted on the return pipe. The instantaneous velocity (u, v, w), corresponding to x (longitudinal), y (lateral), and z (vertical) directions, respectively, was recorded using a Nortek Vectrino Acoustic Doppler Velocimeter (ADV). Spikes in the velocity record were removed by a MATLAB code, which used the acceleration threshold method described in Goring and Nikora (2002). Vertical profiles were measured with a resolution of 1 cm. Four lateral positions between the plant rows were chosen to capture the lateral variation within the canopy. The measurements were first time-averaged, denoted by an overbar, then laterally averaged, denoted by $\langle \rangle_y$, and finally depth-averaged, denoted by $\langle \rangle_z$. Additional details for the velocity measurements can be found in Section 3.3.1 in Xu and Nepf (2020). The velocity was measured at $x = 8$ m (i.e., mid-length along the canopy, Figure 1a). Based on a previous study with the same canopy, the velocity and turbulence were fully developed at 0.58 m from the leading edge. Three water depths (H= 20, 30, and 35 cm) were considered (Table 1). For each water depth, three to four different flow discharges were chosen, producing 10 cases. The channel-average velocity U ranged from 4.8 to 18.5 cm/s, which was consistent with values measured in the field (e.g., Leonard & Luther, 1995; Naden et al., 2006). Plant reconfiguration (bending) was not considered, and for the flow and depth conditions considered here, the model plants did not reconfigure (see discussion in Section 4.5 of Xu & Nepf, 2020). The water surface slope, S, was measured with two wave gauges with 0.2 mm

Table 1
Summary of the Experimental Conditions and Best-Fit Diffusion Scale Factor

Run	H (cm)	$U \pm \sigma_U$ [a] (cm/s)	$\langle a \rangle_z$ [b] (m^{-1})	ϕ	x-Location of SSC measurements (m)	$S \pm \sigma_S$ [c] (10^{-3})	Best-fit α_z at equilibrium
1.1	20	7.6 ± 0.3	3.10	0.0057	1.0, 3.1, 13.2, 14.1	1.3 ± 0.1	2.5
1.2	20	9.4 ± 0.5	3.10	0.0057	0.5, 1.0, 1.9, 3.1, 13.2, 14.1	1.6 ± 0.1	2.0
1.3	20	13.1 ± 0.6	3.10	0.0057	13.2, 14.1	3.6 ± 0.3	2.0
1.4	20	18.5 ± 1.1	3.10	0.0057	13.2, 14.1	7.7 ± 0.5	1.5
2.1	30	6.4 ± 0.3	3.85	0.0064	13.2, 14.1	1.2 ± 0.1	4.0
2.2	30	9.4 ± 0.5	3.85	0.0064	0.5, 1.0, 1.9, 3.1, 13.2, 14.1	2.9 ± 0.2	3.0
2.3	30	13.9 ± 0.6	3.85	0.0064	13.2, 14.1	5.6 ± 0.5	2.5
3.1	35	4.8 ± 0.2	3.94	0.0065	13.2, 14.1	0.8 ± 0.1	3.0
3.2	35	7.6 ± 0.4	3.94	0.0065	1.0, 3.1, 13.2, 14.1	1.9 ± 0.2	3.5
3.3	35	11.4 ± 0.5	3.94	0.0065	13.2, 14.1	3.3 ± 0.2	3.0

[a]Channel-average velocity U determined from the flowmeter was equal to the velocity $\langle \overline{u} \rangle_z$ measured with the ADV. The uncertainty σ_U was associated with fluctuations in the flowmeter reading. [b]Depth-average frontal area per volume $\langle a \rangle_z = mA_f/H$. A_f is the cumulative frontal area of one plant, $A_f = \int_0^H Adz$. [c]Uncertainty in slope σ_s arose from fluctuations in the water surface.

accuracy and 1,000 Hz sampling rate, which were located at $x = 0.5$ and 14.5 m (Table 1 and Supporting Information S1).

The model sediment consisted of silica particles with density $\rho_s = 2.5$ g/cm^3 and median diameter $D_{50} = 29$ μm (Potters Industries). The particle size was chosen to ensure that the sediment could be suspended within the range of possible flow conditions. The particle size distribution (Figure S2) was measured using a Beckman Coulter laser diffraction instrument (Follett & Nepf, 2018). The settling velocity, w_s, was estimated using Equation 4 in Ferguson and Church (2004). For $D_{50} = 29$ μm, $w_{s50} = 0.067$ cm/s (Supporting Information S11). Particles were released at mid-depth and slightly upstream of the canopy, at $x = -0.15$ m (Figure 1a). Before each experiment, 700 g of the particle was mixed with 10 L water to form a dilute solution. The particle slurry was continuously mixed in a 15-L bucket using a magnetic stirrer and injected continuously through a 2-mm nozzle using a peristaltic pump (Figure 1a). A tee-shaped nozzle directed the slurry in the $\pm y$ direction. The slurry discharge rate, Q_{in} was 12.6 ± 1.9 ml/s.

The suspended sediment concentration was measured using four optical backscatter sensors (OBS, Seapoint Sensors Inc.). A prepared slurry concentration, ranging from 0 to 500 mg/L, was used to calibrate the OBS output voltage with concentration (see Supporting Information S3). Pairs of OBSs were mounted on a thin rigid rod (Figure 1a), which moved vertically. SSC was measured simultaneously at two longitudinal positions. A preliminary test experiment was conducted for each flow condition to determine the time at which stationary SSC conditions were reached (Figure S4). The OBS measurement began when the particle release began and measured continuously at 20 Hz for the entire duration of the release (12 min). This time allowed the particles to recirculate in the flume at least twice. The SCC record revealed the time period of the steady state SSC conditions. In subsequent runs with the same flow conditions, the vertical profile of SSC was measured within the steady time-period by vertically moving the rigid rod to obtain measurements at eight vertical positions. Each case was repeated to assess the method's uncertainty. To observe the longitudinal evolution of SSC, multiple experiments were conducted for the same flow condition, with the OBS at different streamwise positions (Table 1).

Fine particles can be captured directly by plant leaves, and other plant surfaces (Kretz et al., 2020). This on-plant sedimentation decreases with increasing flow velocity or collector Reynolds number (Fauria et al., 2015; Purich, 2006; Wingenroth et al., 2021). At the leaf scale, Kretz et al. (2020) observed adaxial pubescence and enhanced sedimentation on leaves. However, for the flow conditions (relatively high flow velocity), plant characteristics (low canopy density and smooth leaves without pubescence), and absence of biofilm in the present study, the on-plant sedimentation was negligible. This was confirmed by the fact that the measured flux of particles in the water column agreed with the injected flux, indicating that deposition of any sort (to the bed or to the plant surfaces) was small enough to be neglected in the experiments.

2.2. Random Displacement Model

A 2D (streamwise, x, and vertical, z) random displacement model was used to simulate the transport of individual particles. Within each time-step, Δt, particles were displaced by time-mean advection in x and turbulent diffusion in z (Gardiner, 2009). Assuming a high streamwise Peclet number, the longitudinal diffusion was neglected (Taylor, 1953). The particle position at the time step $i + 1$ was described as in Tsai et al. (2020):

$$x_{i+1} = x_i + \langle \overline{u}\left(z_i\right)\rangle \Delta t \tag{1}$$

$$z_{i+1} = z_i + \left(\frac{\partial K_z}{\partial z}\left(z_i\right) - w_s\right)\Delta t + \sqrt{2K_z\left(z_i\right)\Delta t}\, R \tag{2}$$

in which K_z is the sediment diffusivity in z. The term $\partial K_z/\partial z$ is a pseudo-velocity needed to prevent the artificial accumulation of particles in the regions of low diffusivity (Durbin, 1983; Wilson & Yee, 2007). R is a random variable with a standard Gaussian distribution (zero mean and unit variance). In this study, the sediment diffusivity K_z was assumed equal to the turbulent diffusivity D_z, since the particles were fine enough for this assumption (Absi, 2010). The time-step, Δt, was chosen so that the vertical particle trajectory within each time-step was much smaller than the scale of vertical gradients in the diffusivity and velocity (Follett et al., 2016; Israelsson et al., 2006). Huai et al. (2019) suggested the length scale $0.05H$ for emergent vegetation.

$$\Delta t < \min\left(\frac{0.05H}{\left|\frac{\partial D_z}{\partial z} - w_s\right|_{\max}}, \frac{\left(0.05H\right)^2}{\left(D_z\right)_{\max}}\right) \tag{3}$$

Simulations with different Δt, ranging from 0.01 to 0.1 s, confirmed that the solution was insensitive to the time step within this range (varied by less than 5%). The time-step was set as 0.05 s.

The measured flux of the suspended particles within the canopy, ($\langle C\rangle_z \cdot W \cdot H \cdot U$), agreed with the injected flux ($C_{in}Q_{in}$) within 10%. This confirmed that no deposition occurred. This was represented in the RDM using a no-flux (reflecting) boundary condition at the channel bottom. The same boundary condition was applied at the water surface, because particles cannot pass through or collect at the surface (Huai et al., 2019; Murphy, 2006):

$$z_i = -z_i, z_i < 0 \quad \left(\text{bottom boundary}\right) \tag{4}$$

$$z_i = 2H - z_i, z_i > H \quad \left(\text{water surface}\right) \tag{5}$$

Within the RDM 10,000 particles were released at the same point that particles entered the canopy in the experiment, and the RDM was run for 6,000 steps (300 s, $\Delta t = 0.05$s), which simulated the duration of the physical experiment. Comparison of the SSC profiles simulated with D_{50} and with a distribution of sizes suggested that D_{50} was a good representative size (Figure S5). Each simulation was repeated for 10 realizations.

To translate the discrete particle positions into a concentration profile, the water depth was divided into $N = 50$ layers, and the concentration, C, was calculated as the number of particles per layer height.

The adaption time, T_a, describes the time-scale needed to reach an equilibrium profile of concentration, defined by the balance of upward diffusion and downward settling. Equilibrium was reached in the RDM when the vertical profile of concentration changes by less than 2% between time-steps. Specifically, the mean percentage error (MPE) summed over the 50 vertical positions was calculated between the current i and previous $i-1$ time-step,

$$\mathrm{MPE}\left(i\right) = \frac{\sum_{j=1}^{N}\frac{\left|C_j\left(i-1\right) - C_j\left(i\right)\right|}{C_j\left(i\right)}}{N} \times 100\% \tag{6}$$

in which $C_j\left(i\right)$ is the sediment concentration in the jth layer at the ith time step. The adaption time, T_a, was defined at the time-point when MPE was less than 2%.

2.3. Parameterization of Transport Parameters in *Typha latifolia*

The RDM was run with the measured velocity profile $\langle \overline{u}\rangle$ and a turbulent diffusion based on the model of Tanino and Nepf (2008). Turbulent diffusivity can be described in terms of a turbulent velocity ($\sqrt{k_t}$) and length-scale (l_t),

$$D = \alpha\sqrt{k_t}\, l_t \tag{7}$$

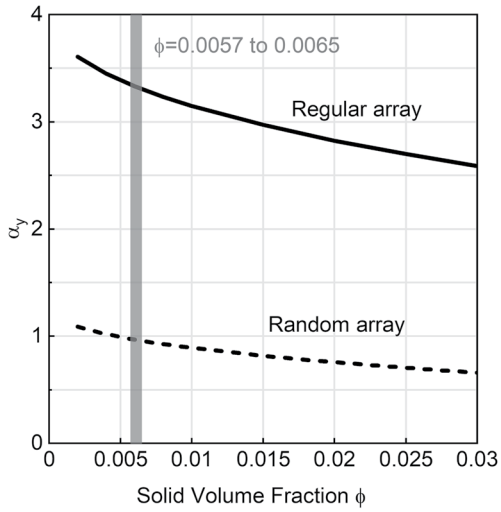

Figure 2. Diffusivity scale constant $\alpha_y = D_y / \sqrt{k_t}\, d$ for lateral turbulent diffusion in an array of cylinders with diameter, d, based on Equation 2.16 and Appendix A in Tanino and Nepf (2008). Solid curve is a regular array with $P_{\mathrm{snc}>2d} = 1$. Dashed curve is for a random array with $P_{\mathrm{snc}>2d}$ described in Equation A21 in Tanino and Nepf (2008). Vertical gray bar indicates the *T. latifolia* canopy in this study, with $\phi = 0.0057$ to 0.0065, Table 1.

in which l_t is the integral length-scale, k_t is the turbulent kinetic energy (TKE) per fluid mass, and α is a scale constant. Within a canopy, l_t, k_t, and α are shaped by vegetation-generated turbulence (e.g., Nepf, 2012). Models for α, l_t and k_t have been developed and validated for an array of rigid, circular cylinders (Tanino & Nepf, 2008). For the *T. latifolia* canopy, l_t equals the culm diameter, d, near the bed and the leaf width, w near the surface, with a smooth transition between (see Equation 16 in Xu & Nepf, 2020, repeated here for convenience).

$$l_t = \begin{cases} d = 1.5, & z < 10 \\ 3.6 - 0.19z, & 10 \le z < 17 \\ w = 0.2 & z \ge 17 \end{cases} \tag{8}$$

All units in Equation 8 are in cm. Note that this relationship represents the average profile measured over many water depths. The turbulent kinetic energy k_t also varies over the *T. latifolia* canopy height (see Equation 17 in Xu & Nepf, 2020),

$$k_t(z) = \gamma^2 \left(C_D \frac{a\, l_t}{2\left(1 - \phi(z)\right)} \right)^{2/3} \langle \overline{u} \rangle^2 \tag{9}$$

in which the frontal area per canopy volume (a, Figure 1c), solid volume fraction (ϕ), and velocity, $\langle \overline{u} \rangle$, are all functions of z. Strictly, Equation 9 should use the form drag coefficient (C_D^{form}, Tanino & Nepf, 2008). However, at typical Reynolds numbers in a canopy, the viscous drag is small compared to the form drag, and $C_D^{\mathrm{form}} \approx 0.9 C_D$ (for plant element $Re > 200$, Etminan et al., 2018), making it reasonable to simplify Equation 9 using $C_D \approx C_D^{\mathrm{form}}$. The scale coefficient for *T. latifolia*, $\gamma^2 = 1.6 \pm 0.4$ (Xu & Nepf, 2020), is slightly larger than that determined for an array of rigid cylinders ($\gamma^2 = 1.1 \pm 0.2$, Equation 3.33 in Tanino, 2008), suggesting that γ^2 may be sensitive to the plant morphology. The present study considered whether predictions of l_t and k_t from Equations 8 and 9 could be used in Equation 7 to predict the turbulent diffusivity within a *T. latifolia* canopy.

For a canopy of cylinders with diameter d and the marsh-relevant solid volume fraction $\phi < 0.03$, the mixing length-scale $l_t = d$, and α depends on both ϕ and the cylinder arrangement (random vs. regular array, Tanino & Nepf, 2008). In particular, α reflects the fraction of canopy space in which the local center-to-center spacing s_{nc} between cylinders is more than $2d$, $P_{s_{nc}>2d}$, because only these regions can support eddies $l_t = d$. For a random array $P_{\mathrm{snc}>2d} = f(\phi)$, but for a staggered or square array in this range, $P_{s_{nc}>2d} = 1$. Note that Tanino and Nepf (2008) considered the lateral diffusivity, which we note with subscript y. The function $\alpha_y = F(\phi)$, based on Equation 2.16 and Appendix A in Tanino and Nepf (2008), is shown in Figure 2. Additional details are provided in Section S7. Within a cylinder array, measured vertical diffusivity has been shown to be smaller than lateral diffusivity, $D_z \approx 0.25 D_y$ for $\phi = 0.006$ to 0.053 (Nepf et al., 1997), which is consistent with the vertical orientation of the array elements. However, field measurements show $D_z \approx D_y$ in *Spartina alterniflora*, which has a morphology similar to *T. latifolia* (Lightbody & Nepf, 2006; Tarrell, 1997). The isotropic diffusion was attributed to the varied orientation of real plant elements.

3. Results and Discussion

3.1. Validation of Vertical Diffusivity Model

3.1.1. Transport of a Neutrally Buoyant Tracer in a Cylinder Array

To validate the diffusivity model (Equations 7–9) and the RDM method, the model was used to simulate a laboratory experiment that measured dye transport (Rhodamine WT) in a cylinder array consisting of two layers of different cylinder densities (Lightbody & Nepf, 2006). The dye was dilute enough to be neutrally buoyant, so that $w_s = 0$ in Equation 2. Cylinders with diameter $d = 0.64$ cm and two lengths were arranged randomly in a predrilled plastic sheet, creating a canopy with two layers: a sparser lower layer with $m_1 = 300$ stems/m^2 and $\phi = 0.0097$, and a denser upper layer with $m_2 = 600$ stems/m^2 and $\phi = 0.0193$ (Figures 4–10

Table 2
Flow Characteristics in Lightbody (2004)

	U (cm/s)		Measured D_z (cm²/s)		Predicted D_z from Equation 7	
H (cm)	Lower layer	Upper layer	Lower layer	Upper layer	Lower layer	Upper layer
20 ± 1	5.2 ± 0.1	3.4 ± 0.1	0.25 ± 0.16	0.04 ± 0.08	0.24 ± 0.08	0.09 ± 0.04

in Lightbody, 2004). The dye was released at mid-width and 0.5 cm from the channel bed. Velocity and dye concentration were measured using an ADV and a Rhodamine fluorometer, respectively. Vertical diffusivity D_z was determined in their study by fitting measured concentration profiles to analytical solutions for vertical concentration profiles (Table 2, the third column).

Based on the Tanino model for a random cylinder array $\alpha_y = 0.90$ and 0.77 for $\phi = 0.0097$ and $\phi = 0.0193$, respectively. For a cylinder array, we expect $\alpha_z = 0.25\alpha_y$, yielding $\alpha_z = 0.23$ and 0.19, respectively. Using these scale factors, the measured k_t, and $l_t = d$ in Equation 7, the vertical diffusivity D_z was predicted to be 0.24 ± 0.08 cm²/s for the lower layer and 0.09 ± 0.04 cm²/s for the upper layer, which agreed with the measured diffusivity within uncertainty (Table 2). Further, this diffusivity accurately predicted the measured concentration profiles. Specifically, 10,000 particles were released at 0.5 cm from the simulated bed, consistent with the experimental setup, and the simulation was run until a steady-state was achieved at four distances from the release ($x = 50$, 100, 200, and 300 cm). The simulation was run 10 times to provide an assessment of the random error. At each longitudinal position, the ensemble average concentration from the 10 realizations agreed with the measured concentration within less than 7.5%, which validated the vertical diffusivity model for a canopy of cylinders (Figure 3a).

3.1.2. Transport of the Suspended Sediment in a Cylinder Array

The diffusivity model and the RDM method were also validated for sediment transport using data from Lu (2008), who measured suspended sediment concentration in a square array of circular cylinders with diameter $d = 0.6$ cm and solid volume fraction $\phi = 0.028$. The plastic particles were 217 μm with $w_s = 0.162$ cm/s. Lu (2008) circulated the particles long enough to obtain an equilibrium SSC profile. They measured the velocity and concentration using an ADV and a siphon, respectively. The velocity was vertically uniform, as expected for a uniform cylinder array (Figures 6 and 7 in Lu, 2008) (Table 3).

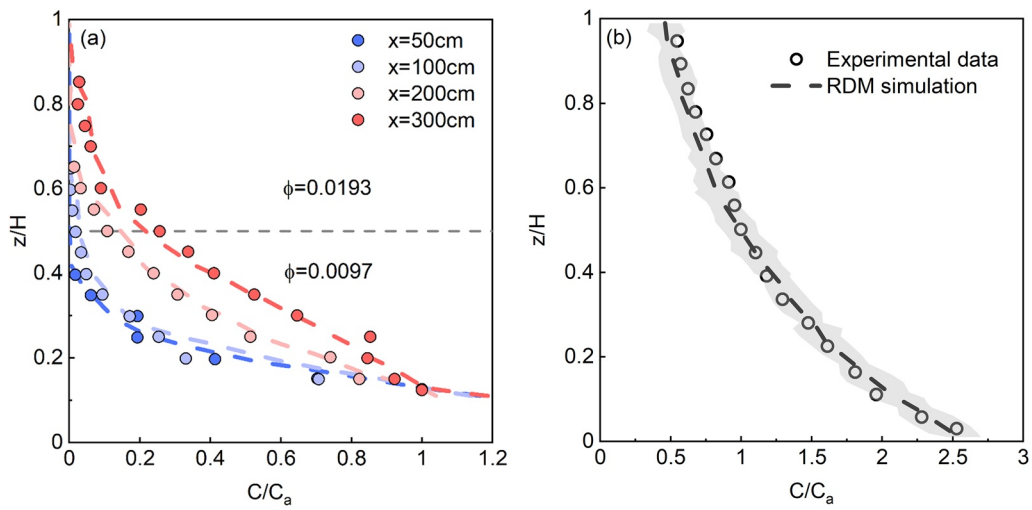

Figure 3. (a) Simulated concentration (dashed lines) and measured concentration (symbols, from Lightbody, 2004). The vertical coordinate was normalized by the water depth, H, and the concentration was normalized by C_a, the reference concentration at $z = 0.1H$. The standard error among 10 realizations ranged from 1% to 4%. The gray dashed line denotes the interface between the two layers. At each position the simulated concentration agreed with the measured concentration within 7.5% (b) Comparison of the equilibrium suspended sediment concentration profile simulated with the random displacement model (RDM) and measured by Lu (2008). The gray area denotes the uncertainty of the RDM results. C_a is the reference concentration at $z = 0.5H$.

Table 3
Flow and Canopy Characteristic in Lu (2008)

Case	H (cm)	U (cm/s)	ϕ	S (10^{-3})	k_t(cm^2/s^2)	α_z	D_z(cm^2/s)
D18-3	18.0	16.9	0.028	13.6	19.9 ± 3.8	0.65	1.7 ± 0.3

The turbulent kinetic energy, $k_t = 19.9 \pm 3.8$ cm^2/s^2, was determined from the measured velocity and Equation 9. For a square array with $\phi = 0.028$, $\alpha_y = 2.6$ (Figure 2), and within a cylinder array we expect $\alpha_z = 0.25\alpha_z = 0.65$. From these estimates, Equation 7 predicted the turbulent diffusion $D_z = 1.7 \pm 0.3$ cm^2/s (standard error propagated from TKE prediction). The equilibrium SSC profile simulated using this predicted diffusivity agreed with the measured profile within the uncertainty (based on standard error among 10 realizations of RDM, gray area in Figure 3b), indicating that the diffusivity prediction (Equation 7) and the RDM method had good performance simulating suspended sediment transport. In conclusion, results presented in this section have validated the vertical diffusivity model for cylinder arrays (Equations 7–9) with both a neutrally buoyant tracer and sediment. However, the extension of this model to more complex morphology must still be considered, which is the motive behind the rest of the study.

3.2. Measured SSC Profiles in the *Typha latifolia* Canopy

The concentration profiles measured at $x = 13.2$ and 14.1 m (open and filled symbols, respectively, Figure 4a) differed by less than 6%, which was comparable to the uncertainty, indicating that the SSC has reached the equilibrium profile by this point. For further analysis, the SSC at these two positions were averaged to represent the equilibrium profiles, which are presented for flow depths $H = 20$ and 35 cm in Figures 4b and 4c, respectively. For comparison, the profile predicted for a bare channel with the same velocity (Rouse profile) was plotted with dashed curves. For the bare channel, the vertical turbulent diffusion has a parabolic distribution (e.g., Cellino, 1998):

$$D_z = \kappa u_* z\left(1 - \frac{z}{H}\right) \tag{10}$$

in which κ (=0.4) is the von Karman constant and u_* is the friction velocity, estimated from the linear distribution of Reynolds stress in the bare channel. For the same channel velocity and depth, SSC profiles in the *T. latifolia* (symbols) differed significantly from the Rouse profile. Within the *T. latifolia*, SSC was close to being vertically uniform in the lower culm region ($z < 15$ cm), which corresponded to nearly the full flow depth for $H = 20$ cm (Figure 4b). With a greater water depth ($H = 35$ cm, Figure 4c), SCC decreased with distance from the bed in the upper region of the canopy ($z > 15$ cm). A more uniform SSC profile in the *T. latifolia*, compared to the bare channel, can be attributed to vegetation-induced turbulence, which increased turbulence intensity by nearly seven-fold, relative to a bare channel with same channel-average velocity (Figure 4e). Further, the shape of the SCC profile can be correlated with the vertical variation in k_t and l_t (Figures 4e and 4f). Specifically, l_t was higher in the lower canopy ($z < 15$ cm), where the turbulence length-scale was set by the culm diameter, compared to the upper canopy ($z > 15$ cm), where l_t was set by the leaf width. Similarly, k_t was higher in the lower canopy ($z < 15$ cm), where the local velocity was higher (Figure 4d). Higher values of k_t and l_t in the lower canopy would be associated with higher values of turbulent diffusivity (Equation 7), which was consistent with a more uniform SSC in the lower region of the canopy, compared to the upper canopy (Figure 4c).

The vertical distribution for SSC became more uniform as the channel-average velocity increased (Figure 4c). Specifically, the bed to surface concentration difference decreased from 0.71 to 0.36 as the velocity increased from 4.8 cm/s (blue dots, Case 3.1) to 11.4 cm/s (red dots, Case 3.3). This suggested that vertical diffusivity increased with velocity, which was consistent with the scaling $D_z \sim \sqrt{k_t} \sim U$. For $H = 20$ cm, a velocity dependence was not observed (Figure 4b), because in each of these cases the diffusivity was high enough to produce an essentially uniform SSC profile. For example, the depth-average diffusivity, $\langle D_z \rangle_z = 5.6$ cm^2/s, for Case 1.1 was higher than the value, $\langle D_z \rangle_z = 2.9$ cm^2/s, for Case 3.1. Furthermore, the diffusivity profile was much more uniform over depth for $H = 20$ cm (Case 1.1, Figure 6b) than for $H = 35$ cm (Case 3.1, Figure 6d).

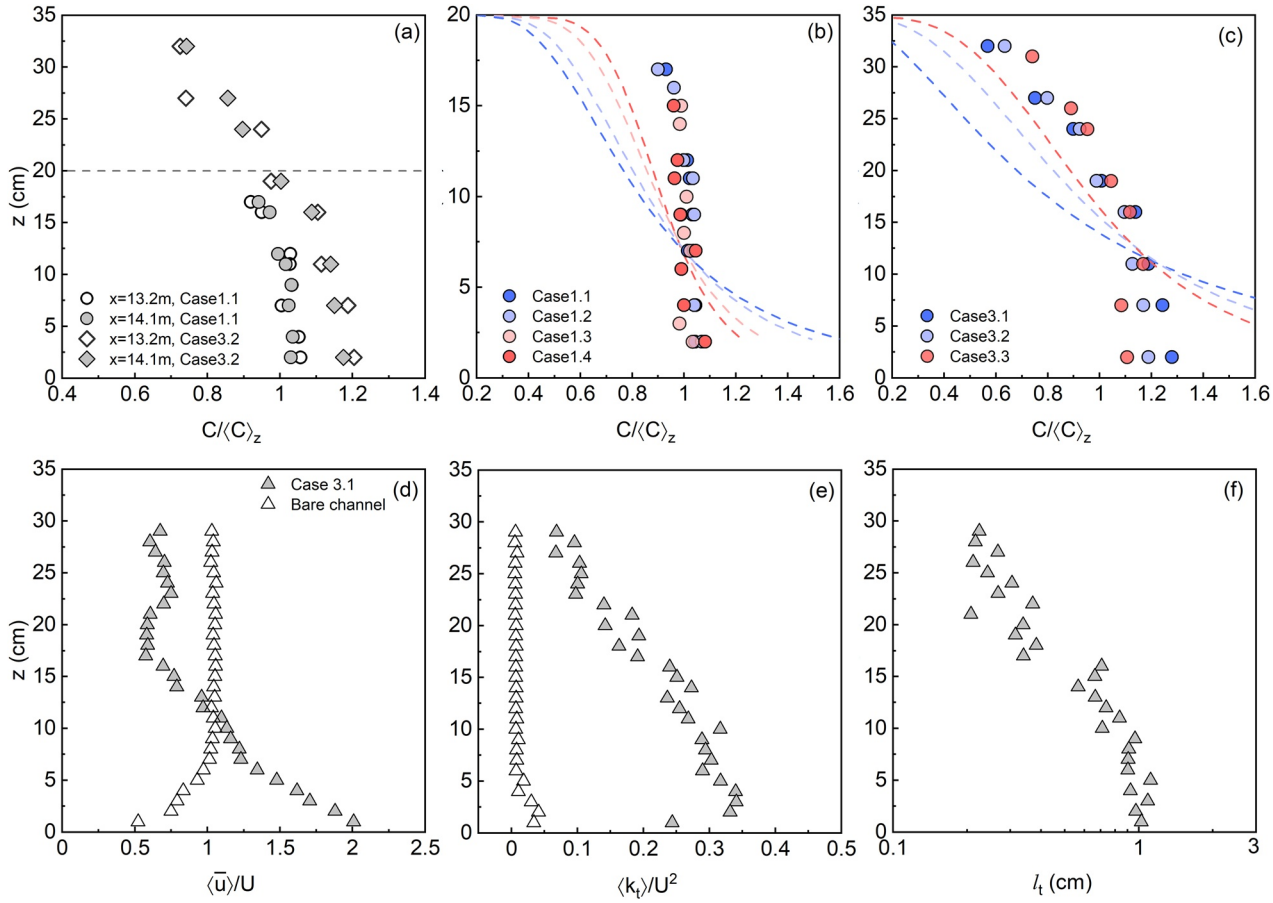

Figure 4. (a) Suspended sediment concentration (SSC) within *T. latifolia* canopy at $x = 13.2$ m (open symbols) and 14.1 m (filled symbols) for Case1.1 (circles, $H = 20$ cm, $U = 7.6$ cm/s) and Case3.2 (diamonds, $H = 35$ cm, $U = 7.6$ cm/s). Subplots (b and c) show equilibrium SSC profiles in *T. latifolia* for (b) $H = 20$ cm and (c) $H = 35$ cm. The dashed lines show the SSC profile in the bare channel estimated using the Rouse formula. (d) Measured values of velocity, $\langle \overline{u} \rangle$, and (e) measured turbulent kinetic energy, $\langle k_t \rangle$, each normalized by the channel average velocity U, and (f) integral length-scale, l_t for Case 3.1, with $H = 35$ cm. Open triangles represent the bare channel with the same flow condition (legend in subplot d).

3.3. Canopy Drag Coefficient

The *T. latifolia* drag coefficient, C_D, is needed to predict k_t and thus the turbulent diffusivity (Equations 7 and 9). The drag coefficient was estimated from the momentum balance and measured water surface slope S (Table 1). In sparse, emergent canopies, viscous, Reynolds, and dispersive stresses are typically much smaller than canopy drag (Lightbody & Nepf, 2006; Xu & Nepf, 2020), so that the momentum equation for the fully developed, steady flow can be simplified to a balance of canopy drag and pressure.

$$0 = \underbrace{gS}_{\substack{\text{pressure} \\ \text{forcing term}}} \quad \underbrace{-\frac{1}{2}\frac{C_D a}{(1-\phi)}U^2}_{\substack{\text{vegetation} \\ \text{drag}}} \tag{11}$$

Xu and Nepf (2020) determined a drag coefficient for an individual plant using a force transducer to measure the drag on an individual plant within a canopy. To explore whether this plant-scale drag coefficient represents the distributed drag within a canopy (canopy-scale drag coefficient, based on Equation 11), C_D values estimated by the two methods are compared in Figure 5. The plant-scale C_D agreed with the canopy-scale C_D to be within 10%, and C_D(plant-scale) = 1.04 ± 0.06 C_D(canopy-scale), indicating that C_D estimated by Equation 11 and C_D measured on an individual plant were interchangeable. This indicated that the drag (energy loss) associated with shear generated in the spaces between the plants was negligible. This supports the application of the plant-scale drag for use in distributed drag models.

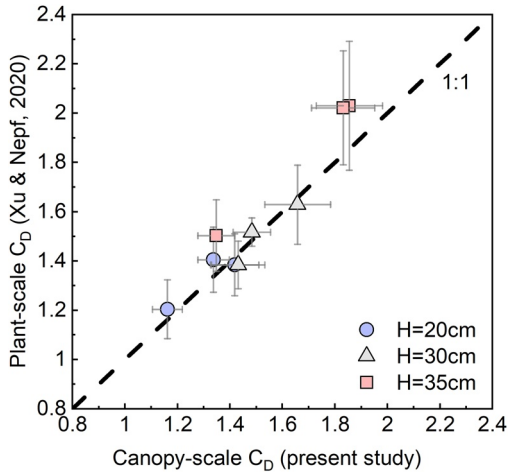

Figure 5. Comparison of canopy-scale C_D, determined from Equation 11, and plant-scale C_D, based on force measured on an individual plant within a canopy (from Xu & Nepf, 2020). The horizontal error bars arise from the uncertainty of the water surface slope. The vertical error bars are associated with replicate measurements of force on the individual plant. The dashed line represents the 1:1 line.

3.4. Diffusivity in a *Typha latifolia* Canopy

The SSC profile was simulated using the RDM with a range of diffusivity scale factors in Equation 7, $\alpha_z = 0.5$ to 4.0, and these were compared to the measured profiles (Figures 6a and 6c). As α_z increased, the simulated SSC decreased near the bed and increased in upper canopy, consistent with an increase in the vertical turbulent diffusion. The difference between the simulated and measured SSC was quantified with the mean percentage error (Equation 6, inset graphs in Figure 6). The trend of MPE with α_z was similar for all cases (Figure S7), decreasing rapidly between $\alpha_z = 0.5$ and 1, and reaching a minimum error of 1.2%–4.8% for α_z between 1.5 and 4 (Table 1). The best-fit α_z differed with water depth. For $H = 20$ cm, best-fit α_z ranged from 1.5 to 2.5, with mean 2.0 ± 0.4. For $H = 30$ and 35 cm, best-fit α_z ranged from 2.5 to 4.0, with mean 3.1 ± 0.5. There was no dependence of α_z on velocity (Table 1), which was consistent with Tanino's description of α_z as a function of canopy morphology and the fact that no reconfiguration was observed (Section 2.3 in Tanino & Nepf, 2008).

The profile of vertical diffusivity D_z corresponding to the best-fit α_z is presented in Figures 6b and 6d. The diffusivity in a bare channel (Equation 10) with the same channel velocity was included with a dashed curve, which illustrated the significant degree to which the canopy enhanced the vertical diffusivity. For example, in Cases 1.1 and 3.1, the depth-average D_z with *T. latifolia* was 5–10 times higher than that for bare channel. The canopy also changed the shape of the diffusivity profile. The diffusivity was highest in the culm region near the bed, corresponding to the region of maximum turbulent kinetic energy k_t and integral length-scale l_t (Figures 4e and 4f). However, it is worth noting that the comparison in the present study assumed the same velocity in the vegetated and bare channel, whereas in reality the velocity will be lower in the vegetation. For a fixed water surface slope driving flow into the vegetation, velocity decreases with increasing stem density. The decreasing velocity dominates the augmented turbulence generation (Equation 9), such that turbulence decreases with increasing stem density (see Figure 4 in Yang & Nepf, 2018), from which Equation 7 predicts a decrease in vertical diffusivity with increasing stem density.

To further explore the diffusivity model, the streamwise evolution of SSC profiles was simulated and compared to the measured concentration at $x = 0.5$, 1.0, 1.9, 3.1 m. (Figure S9). Because the evolving SSC profiles involved a wider range of sediment vertical distribution, it provided a more robust assessment of best-fit α_z (Table 4). For the smallest depth (occupied mostly by the culm), the best-fit α_z based on SSC spatial evolution was $\alpha_z = 1.0 \pm 0.4$, which was smaller than that inferred from equilibrium SSC, $\alpha_z = 2.0 \pm 0.4$. However, for the larger depths (which included both the culm and leaves), the best-fit from SSC spatial evolution, $\alpha_z = 2.8 \pm 0.6$, was the same within uncertainty to that based on the equilibrium profile, $\alpha_z = 3.1 \pm 0.5$.

The fitted α_z values fell within the expected values based on the modified Tanino model, suggesting that this model can predict α_z for natural canopies Specifically, the culm region of the canopy (Figure 7a), has a geometry similar to a staggered array of vertical cylinders. For a staggered array of cylinders, previous studies have shown $\alpha_z \approx 0.25\alpha_y$ (Nepf et al., 1997), and for $\phi = 0.0057$ (Table 1) $\alpha_y = 3.3$ (Figure 2), such that $\alpha_z = 0.25\alpha_y = 0.83$. Considering only profiles for which the particle plume was isolated within the culm region (plume height <20 cm in Table 4), the best-fit values yielded the average $\alpha_z = 0.75 \pm 0.14$ (Table 4), which agreed with the model prediction. When the water depth was larger ($H = 30$ and 35 cm), the sediment interacted with the upper canopy of leaves with varied orientation, for which previous studies have suggested $D_z \approx D_y$ (Lightbody & Nepf, 2006; Nepf, 1999). Then, from Figure 2, we predict $\alpha_z = \alpha_y = 3.3$. Considering the profiles for which the sediment interacted with the upper canopy (plume height >20 cm), the average $\alpha_z = 2.9 \pm 0.2$ (Table 4), which was close to the predicted value ($\alpha_z = 3.3$). This agreement supports the hypothesis in Lightbody and Nepf (2006) that leaves with varied orientation generate an isotropic turbulent diffusion ($D_z \approx D_y$). Further, the best-fit α_z increased with increasing plume height, consistent with an increasing contribution of the leaf region (Figure 7c). These observations suggested that

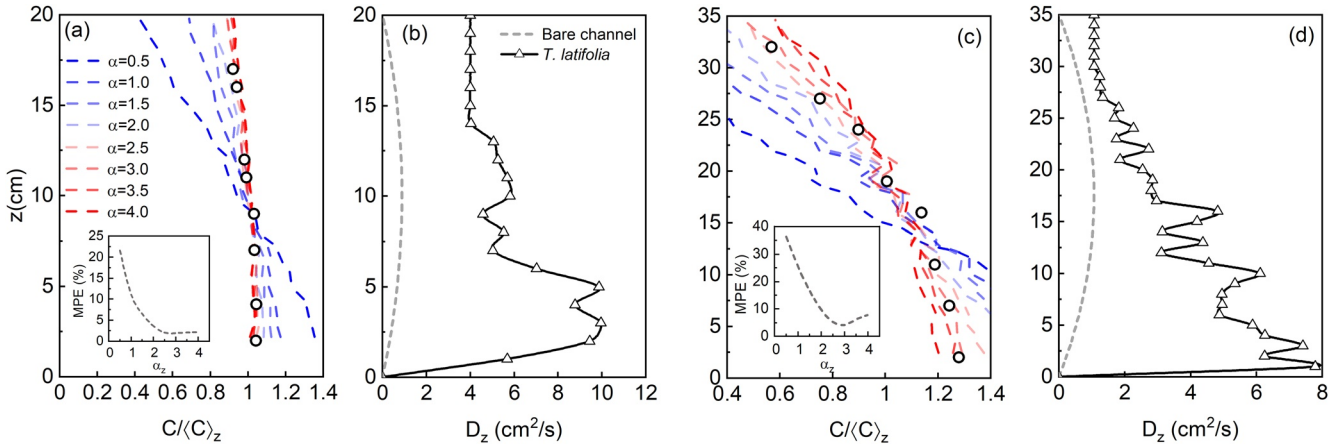

Figure 6. Subplots (a) and (c) compare the measured equilibrium suspended sediment concentration profile (open circle) and random displacement model simulation (dashed lines, from blue to red $\alpha_z = 0.5$ to 4). Concentration is normalized by the depth-average $\langle C \rangle_z$. (a) Case 1.1: $H = 20$ cm, $U = 7.6$ cm/s, (c) Case 3.1: $H = 35$ cm, $U = 4.8$ cm/s (legend in subplot a). Inset graph shows mean percentage error between the measured and simulated concentration as a function of α_z. Subplots (b and d) are vertical profiles of diffusivity using best-fit α_z in the *T. latifolia* canopy (open triangle) and bare channel (Equation 10, dashed lines) for (b) Case 1.1 and (d) Case 3.1 (legend in subplot b).

the diffusion scale factor had a dependence on water depth, due to the range of morphology included for different depths. The following values of α_z, dependent on water depth, are recommended for the *T. latifolia* canopy (also dashed lines in Figure 7c).

$$\alpha_z = \begin{cases} 0.25\alpha_y, & H < 15\,cm \quad (\text{culm}) \\ (0.08H - 0.9)\alpha_y, & 15\,cm \le H < 25\,cm\,(\text{transtion}) \\ \alpha_y & H \ge 25\,cm \quad (\text{leaves}) \end{cases} \tag{12}$$

The three regions (culm, transition, leaves) were distinguished by three linear regions within the profile of the frontal area of *T. latifolia* (red lines in Figure 7b). To apply this profile to other canopies, one would need to identify the vertical extend of the culm-dominated and leaf-dominated regions based on plant morphology. Note that Equation 12 defines a constant value of α_z as a function of water depth (H), but we also considered the impact of α_z variation over depth (z). However, this additional level of detail did not significantly impact the simulation (see Figure S10), indicating that a constant $\alpha_z = f(H)$ is adequate for representing the vertical variation in diffusivity (Equation 7).

3.5. Adaption Time of SSC in *Typha latifolia* Canopy

When water carrying the suspended sediment enters a marsh, the SSC profile adjusts to the new vegetated flow condition. It is useful to know the time-scale for this adjustment, called the adaption time, as this predicts the distance from the marsh edge that a new equilibrium SSC profile will evolve, $X_a = U T_a$. In addition, this provides guidance for choosing the run time for numerical simulations. The adaptation time was determined from the RDM using the mean percentage error (MPE, Equation 6) in the concentration profile. At each time step the MPE of SSC at the current i and previous $i - 1$ time step was calculated. When

Table 4
Best-Fit α_z Based on Spatial Evolution and Equilibrium Suspended Sediment Concentration Profile

Run	H(cm)	Distance from the leading edge (m)	Top of the particle plume (cm)	Best-fit α_z at corresponding x	Best-fit α_z at equilibrium
1.1	20	1.0, 3.1	13, 20	0.5, 1.5	2.5
1.2	20	0.5, 1.0, 1.9, 3.1	11, 15, 18, 20	0.5, 1.0, 1.0, 1.5	2.0
2.2	30	0.5, 1.0, 1.9, 3.1	25, 30, 30, 30	3.0, 3.0, 2.0, 2.0	3.0
3.2	35	1.0, 3.1	32, 34	3.5, 3.0	3.5

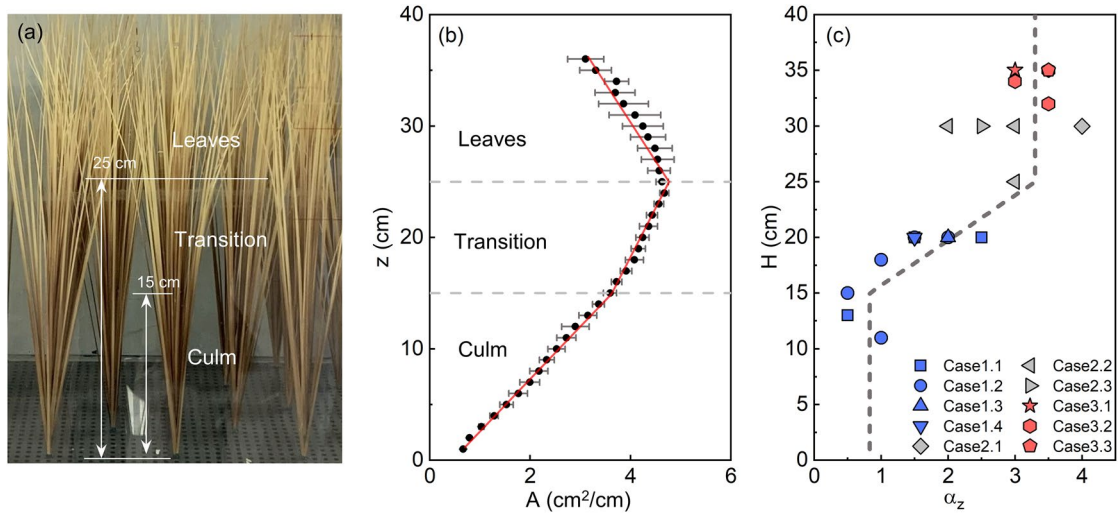

Figure 7. (a) Definition of morphology regions within a *T. latifolia* canopy. Near the bed, leaves are tightly clustered in culms, resembling vertical cylinders. Near the top of the canopy, leaves have varied orientation. (b) Vertical profile of the *T. latifolia* frontal area per cm vertical interval, A (cm^2/cm), shown with black dots. Three regions were distinguished by linear regions within the frontal area profile, shown with red lines. (c) The vertical diffusion scale factor α_z varied with water depth. The dashed lines are Equation 12. The blue, gray, and red symbols are the best-fit α_z from RDM simulations with H = 20, 30, and 35 cm, respectively. The vertical position of each symbol corresponds to the top of the plume (i.e., Table 4), reflecting the depth over which the plume has been mixed, and thus the vertical domain over which diffusivity has acted on the plume.

MPE was less than 2%, the SSC was assumed to reach the equilibrium state and this was defined the adaptation time, T_a.

For channels without vegetation and fine sediment (small sediment Peclet Number, $P_e = w_s H/D_z < 1$), previous studies have found T_a scales with the diffusivity and water depth (Chatwin, 1972; Fischer, 1973; Prandle, 1997; Pritchard, 2006),

$$T_a = \beta \frac{H^2}{\langle D_z \rangle_z} \tag{13}$$

in which $\langle D_z \rangle_z$ is the depth-averaged vertical diffusivity and β is a scale coefficient. The RDM simulations indicated that the same scaling also applied within the *T. latifolia* canopy (Figure 8), with $\beta = 0.41 \pm 0.09$, which was consistent with the value of β suggested in Fischer (1973). For coarse particles (large P_e), the adaption time-scale would be set by the settling time, $T_a \sim H/w_s$ (Pritchard, 2006), since the gravity of the particle would dominate the adaption process.

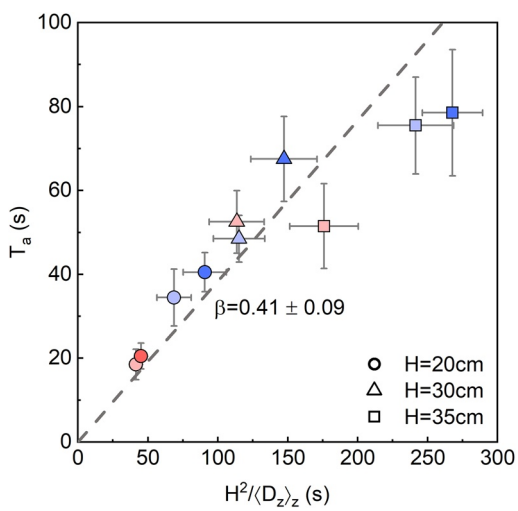

Figure 8. Comparison between the adaptation time T_a and diffusion time-scale $H^2/\langle D_z \rangle_z$. Blue to red colors represent increasing velocity U. The vertical error bars reflect the standard error among 10 RDM simulations. The horizontal error bars arise from the spatial variation in $\langle D_z \rangle_z$ The dashed line is the fitting curve $T_a = 0.41\ H^2/\langle D_z \rangle_z$.

3.6. Model Application

Together with Xu and Nepf (2020), the present study provides a way to model vertical diffusivity within a canopy of emergent vegetation. This could be used to estimate the adaptation time-scale (Equation 13) and associated adaptation distance, which can be used to predict or interpret deposition patterns within marshes. The diffusivity can also be used within an RDM or a field-scale simulation tool (e.g., Delft-3D) to predict the fate of the suspended sediment within a marsh. The model requires a characterization of the plant frontal area profile, A(z) (e.g., see image analysis described in Figure 1 of Xu & Nepf, 2020, and Figure 7), and the plant area density (m), culm diameter (d) and leaf width (w). These plant geometric parameters defined the vertical profiles of $a = mA$ and l_t (as in Equation 8). The vertical profile of the velocity, $\langle \overline{u} \rangle$, can be inferred from Equation 11, or from the hydrodynamic simulation. Equation 9 estimates

the turbulent kinetic energy, k_t. The diffusivity scale constants α_y and α_z are estimated from the solid volume fraction (Figure 2) and water depth (Equation 12). The vertical profile of the vertical diffusivity, D_z, is then estimated from Equation 7. We note that, at the field scale the plant geometric parameters (A, m, d, and w) can vary in the horizontal plane. Because velocity and turbulence adjust over fairly short distances (a few water depths) within emergent canopies (Figure 4 in Xu & Nepf, 2020), the turbulent diffusivity (Equation 7) will also adjust quickly. This means that the model for turbulent diffusivity described in the present paper could be used to model spatial variation in diffusivity across scales of canopy variation, if the spatial distributions of A, m, d, and w are known.

4. Conclusion

The presence of vegetation alters the vertical structure of the mean and turbulent velocity, and these changes impact the vertical diffusivity and the suspended sediment profiles. Compared to conditions without vegetation, but the same velocity, the vertically diffusivity within a *T. latifolia* canopy was both larger and exhibited a vertical variation correlated with plant morphology, both of which can be attributed to vegetation-generated turbulence. Specifically, vegetated-generated diffusivity was higher in the culm region near the bed, and decreased in the upper canopy, dominated by distributed leaves. Correlated to this, the SSC profile in the lower region of the canopy was nearly uniform, while in upper region the concentration decreased with distance from the bed. Drawing on existing models for stem-generated turbulence, a model for vertical diffusivity was validated with tracer data within cylinder arrays and then modified to reflect the specific morphology of the *T. latifolia* canopy. RDM simulations using the modified diffusivity model produced good agreement with the measured suspended sediment concentration. The new diffusivity model can be used to improve prediction of the sediment's fate in marsh systems.

Data Availability Statement

The data used to generate key figures in this study are available through Figshare at this site (https://doi.org/10.6084/m9.figshare.14123651).

Acknowledgments
This study received support from the Gulf Research Program and US NSF Grant EAR 1854564. Any opinions, findings, and conclusions in this study are those of the author(s) and do not necessarily reflect the views of the funding agencies. Y. Xu was supported by the National Natural Science Foundation of China (51879138). The authors thank Elizabeth Follett for her great assistance with the numerical model. The authors thank Rachel Schaefer for her great assistance with the experiments and Danxun Li for his insightful discussions.

References

Absi, R. (2010). Concentration profiles for fine and coarse sediments suspended by waves over ripples: An analytical study with the 1-DV gradient diffusion model. *Advances in Water Resources*, *33*(4), 411–418. https://doi.org/10.1016/j.advwatres.2010.01.006

Barbier, E. B., Hacker, S. D., Kennedy, C., Koch, E. W., Stier, A. C., & Silliman, B. R. (2011). The value of estuarine and coastal ecosystem services. *Ecological Monographs*, *81*(2), 169–193. https://doi.org/10.1890/10-1510.1

Cellino, M. (1998). *Experimental study of suspension flow in open channels* (PhD thesis). Lausanne, CHE: Ecole Polytechnique Fédérale de Lausanne. https://doi.org/10.5075/epfl-thesis-1824

Chatwin, P. C. (1972). The cumulants of the distribution of concentration of a solute dispersing in solvent flowing through a tube. *Journal of Fluid Mechanics*, *51*(1), 63–67. https://doi.org/10.1017/S0022112072001077

Coleman, N. L. (1986). Effects of Suspended sediment on the open-channel velocity distribution. *Water Resources Research*, *22*(10), 1377–1384. https://doi.org/10.1029/WR022i010p01377

Costanza, R., d'Arge, R., de Groot, R., Farber, S., Grasso, M., Hannon, B., et al. (1997). The value of the world's ecosystem services and natural capital. *Nature*, *387*(6630), 253–260. https://doi.org/10.1038/387253a0

Durbin, P. A. (1983). *Stochastic differential equations and turbulent dispersion*. NASA reference Publication 1103. Retrieved from https://ntrs.nasa.gov/search.jsp?R=19830014275

Etminan, V., Ghisalberti, M., & Lowe, R. J. (2018). Predicting bed shear stresses in vegetated channels. *Water Resources Research*, *54*(11), 9187–9206. https://doi.org/10.1029/2018WR022811

Fauria, K. E., Kerwin, R. E., Nover, D., & Schladow, S. G. (2015). Suspended particle capture by synthetic vegetation in a laboratory flume. *Water Resources Research*, *51*(11), 9112–9126. https://doi.org/10.1002/2014WR016481

Ferguson, R. I., & Church, M. (2004). A simple universal equation for grain settling velocity. *Journal of Sedimentary Research*, *74*(6), 933–937. https://doi.org/10.1306/051204740933

Fischer, H. B. (1973). Longitudinal dispersion and turbulent mixing in open-channel flow. *Annual Review of Fluid Mechanics*, *5*(1), 59–78. https://doi.org/10.1146/annurev.fl.05.010173.000423

Follett, E., Chamecki, M., & Nepf, H. (2016). Evaluation of a random displacement model for predicting particle escape from canopies using a simple eddy diffusivity model. *Agricultural and Forest Meteorology*, *224*, 40–48. https://doi.org/10.1016/j.agrformet.2016.04.004

Follett, E., & Nepf, H. (2018). Particle retention in a submerged meadow and its variation near the leading edge. *Estuaries and Coasts*, *41*(3), 724–733. https://doi.org/10.1007/s12237-017-0305-3

Fourqurean, J. W., Duarte, C. M., Kennedy, H., Marbà, N., Holmer, M., Mateo, M. A., et al. (2012). Seagrass ecosystems as a globally significant carbon stock. *Nature Geoscience*, *5*(7), 505–509. https://doi.org/10.1038/ngeo1477

Gardiner, C. (2009). Stochastic Methods (Vol. 4). Berlin: Springer.

Goring, D. G., & Nikora, V. I. (2002). Despiking acoustic Doppler velocimeter data. *Journal of Hydraulic Engineering*, *128*(1), 117–126. https://doi.org/10.1061/(ASCE)0733-9429(2002)128:1(117)

Huai, W., Yang, L., Wang, W.-J., Guo, Y., Wang, T., & Cheng, Y. (2019). Predicting the vertical low suspended sediment concentration in vegetated flow using a random displacement model. *Journal of Hydrology*, *578*, 124101. https://doi.org/10.1016/j.jhydrol.2019.124101
Israelsson, P. H., Kim, Y. D., & Adams, E. E. (2006). A comparison of three Lagrangian approaches for extending near field mixing calculations. *Environmental Modelling & Software*, *21*(12), 1631–1649. https://doi.org/10.1016/j.envsoft.2005.07.008
Jiménez, J. (2012). Cascades in wall-bounded turbulence. *Annual Review of Fluid Mechanics*, *44*(1), 27–45. https://doi.org/10.1146/annurev-fluid-120710-101039
Kemp, J. L., Harper, D. M., & Crosa, G. A. (2000). The habitat-scale ecohydraulics of rivers. *Ecological Engineering*, *16*(1), 17–29. https://doi.org/10.1016/S0925-8574(00)00073-2
Kretz, L., Seele, C., van der Plas, F., Weigelt, A., & Wirth, C. (2020). Leaf area and pubescence drive sedimentation on leaf surfaces during flooding. *Oecologia*, *193*(3), 535–545. https://doi.org/10.1007/s00442-020-04664-2
Leonard, L. A., & Luther, M. E. (1995). Flow hydrodynamics in tidal marsh canopies. *Limnology and Oceanography*, *40*(8), 1474–1484. https://doi.org/10.4319/lo.1995.40.8.1474
Li, Y., Xie, L., & Su, T. C. (2020). Profile of suspended sediment concentration in submerged vegetated shallow water flow. *Water Resources Research*, *56*(4), e2019WR025551. https://doi.org/10.1029/2019WR025551
Lightbody, A. F. (2004). *Field and laboratory observations of small-scale dispersion in wetlands* (MS thesis). MA, USA: Massachusetts Institute of Technology.
Lightbody, A. F., & Nepf, H. M. (2006). Prediction of velocity profiles and longitudinal dispersion in salt marsh vegetation. *Limnology and Oceanography*, *51*(1), 218–228. https://doi.org/10.4319/lo.2006.51.1.0218
Liu, J., Zhang, Z., Yu, Z., Liang, Y., Li, X., & Ren, L. (2017). The structure and flexural properties of *Typha* leaves. *Applied Bionics and Biomechanics*, *2017*, 1–9. https://doi.org/10.1155/2017/1249870
Lu, S. Q. (2008). *Experimental study on suspended sediment distribution in flow with rigid vegetation* (PhD thesis). Jiangsu, CN: Hohai University. (in Chinese).
Minderhoud, P. S. J., Coumou, L., Erkens, G., Middelkoop, H., & Stouthamer, E. (2019). Mekong delta much lower than previously assumed in sea-level rise impact assessments. *Nature Communications*, *10*(1), 3847. https://doi.org/10.1038/s41467-019-11602-1
Murphy, E. (2006). *Longitudinal dispersion in vegetated flow* (MS thesis). MA, USA: Massachusetts Institute of Technology.
Naden, P., Rameshwaran, P., Mountford, O., & Robertson, C. (2006). The influence of macrophyte growth, typical of eutrophic conditions, on river flow velocities and turbulence production. *Hydrological Processes*, *20*(18), 3915–3938. https://doi.org/10.1002/hyp.6165
Nepf, H. M. (1999). Drag, turbulence, and diffusion in flow through emergent vegetation. *Water Resources Research*, *35*(2), 479–489. https://doi.org/10.1029/1998WR900069
Nepf, H. M. (2012). Flow and transport in regions with aquatic vegetation. *Annual Review of Fluid Mechanics*, *44*(1), 123–142. https://doi.org/10.1146/annurev-fluid-120710-101048
Nepf, H. M., Sullivan, J. A., & Zavistoski, R. A. (1997). A model for diffusion within emergent vegetation. *Limnology and Oceanography*, *42*(8), 1735–1745. https://doi.org/10.4319/lo.1997.42.8.1735
Nittrouer, J. A., Best, J. L., Brantley, C., Cash, R. W., Czapiga, M., Kumar, P., & Parker, G. (2012). Mitigating land loss in coastal Louisiana by controlled diversion of Mississippi River sand. *Nature Geoscience*, *5*(8), 534–537. https://doi.org/10.1038/ngeo1525
Prandle, D. (1997). Tidal characteristics of suspended sediment concentrations. *Journal of Hydraulic Engineering*, *123*(4), 341–350. https://doi.org/10.1061/(ASCE)0733-9429(1997)123:4(341)
Pritchard, D. (2006). Rate of deposition of fine sediment from suspension. *Journal of Hydraulic Engineering*, *132*(5), 533–536. https://doi.org/10.1061/(ASCE)0733-9429(2006)132:5(533)
Purich, A. (2006). *The capture of suspended particles by aquatic vegetation* (PhD thesis). Perth, AUS: University of Western Australia.
Rouse, H. (1937). Modern conceptions of the mechanics of fluid turbulence. *Transactions of the American Society of Civil Engineers*, *102*, 463–505. https://doi.org/10.1061/taceat.0004872
Tanino, Y. (2008). *Flow and solute transport in random cylinder arrays: A model for emergent aquatic plant canopies* (PhD thesis). MA, USA: Massachusetts Institute of Technology.
Tanino, Y., & Nepf, H. M. (2008). Lateral dispersion in random cylinder arrays at high Reynolds number. *Journal of Fluid Mechanics*, *600*, 339–371. https://doi.org/10.1017/S0022112008000505
Tarrell, A. E. (1997). *A field investigation of diffusion within a submerged plant canopy* (MS thesis). MA, USA: Massachusetts Institute of Technology and Woods Hole Oceanographic Institution. https://doi.org/10.1575/1912/5667
Taylor, G. I. (1953). Dispersion of soluble matter in solvent flowing slowly through a tube. *Proceedings of the Royal Society of London. Series A. Mathematical and Physical Sciences*, *219*(1137), 186–203. https://doi.org/10.1098/rspa.1953.0139
Tinoco, R. O. (2011). *An experimental investigation of drag and the turbulent flow structure in simulated and real aquatic vegetation* (PhD thesis). NY, USA: Cornell University.
Tsai, C. W., Hung, S. Y., & Wu, T.-H. (2020). Stochastic sediment transport: Anomalous diffusions and random movement. *Stochastic Environmental Research and Risk Assessment*, *34*(2), 397–413. https://doi.org/10.1007/s00477-020-01775-3
Tseng, C., & Tinoco, R. O. (2020). A two-layer turbulence-based model to predict suspended sediment concentration in flows with aquatic vegetation. *Geophysical Research Letters*, *48*. https://doi.org/10.1029/2020GL091255
Wilson, J. D., & Yee, E. (2007). A critical examination of the random displacement model of turbulent dispersion. *Boundary-Layer Meteorology*, *125*(3), 399–416. https://doi.org/10.1007/s10546-007-9201-x
Wingenroth, J., Yee, C., Nghiem, J., & Larsen, L. (2021). Effects of stem density and Reynolds number on fine sediment interception by emergent vegetation. *Geosciences*, *11*(3), 136. https://doi.org/10.3390/geosciences11030136
Xu, Y., & Nepf, H. (2020). Measured and predicted turbulent kinetic energy in flow through emergent vegetation with real plant morphology. *Water Resources Research*, *56*(12), e2020WR027892. https://doi.org/10.1029/2020WR027892
Yang, J. Q., & Nepf, H. M. (2018). A turbulence-based bed-load transport model for bare and vegetated channels. *Geophysical Research Letters*, *45*(19), 10428–10436. https://doi.org/10.1029/2018GL079319
Zhang, Y., Lai, X., Ma, J., Zhang, Q., Yu, R., Yao, X., & Deng, H. (2021). Field study on flow structures within aquatic vegetation under combined currents and small-scale waves. *Hydrological Processes*, *35*(4). https://doi.org/10.1002/hyp.14121